2021 43rd Annual International Conference of the
IEEE Engineering in Medicine & Biology Society (EMBC)
Oct 31 - Nov 4, 2021. Virtual Conference

Simulation of SAR Induced Heating in Infants undergoing 1.5 T Magnetic Resonance Imaging

Robert Kowal[1,4], Marcus Prier[2,4], Enrico Pannicke[3,4], Ralf Vick[3], Georg Rose[1,4], Oliver Speck[2,4]

***Abstract*— RF absorption in patients undergoing MRI procedures poses a major safety risk due to resulting heating in the tissue. In order to stay below permitted temperature limits the SAR has to be quantified and limited. Based on the model of an infant inside a birdcage coil we have investigated the SAR distribution in the body at $1.5\,\mathrm{T}$. Thermal simulations could thus be performed to establish a relationship between the limitations of SAR and temperature. Results show a thermal hotspot in the neck region caused by high local absorption. The temperature limits in this local area were exceeded after $7\,\mathrm{min}$ of excitation within regulatory SAR limits. For a long-term exposure critical organs in the body's core also undergo thermal stress beyond limitations. This indicates the need for constraints in regard to long MR procedures to consider the temporal aspect of heating.**

***Clinical relevance*—This work establishes a relationship between SAR and temperature in infants undergoing MRI and shows potential risks of long-term procedures due to induced thermal stress.**

I. INTRODUCTION

The diagnostic method of magnetic resonance imaging (MRI) is a well-established technique for the visualization of a wide range of diseases and is recommended for use in numerous diagnoses on neonates and infants [1], [2]. Due to its advantages of high resolution combined with excellent soft tissue contrast, this method stands out from the alternatives like ultrasound or computed tomography. With regard to these young patients, the absence of ionizing radiation is of particular importance, as potential long-term radiation damage is avoided.

During an MRI scan, the patient is exposed to radio frequency (RF) pulses, which are essential for imaging but have the side effect of causing unwanted energy absorption and induced heating of the tissue. This power can be quantified by the specific absorption rate (SAR). To ensure a low-risk examination, the SAR as well as the temperatures are generally limited by standards [3]. Compliance with these SAR limits is intended to ensure that no temperature limits are exceeded which may cause physiological or sensory effects.

In this work, the temperature rise in the body of an infant as a result of the excitation with a dedicated birdcage coil at $1.5\,\mathrm{T}$ is investigated. The formation of local skin temperature hotspots, as well as critical organs, are monitored with respect to the applicable SAR limits.

[1] Robert Kowal and Georg Rose are with the Chair in Healthcare Telematics and Medical Engineering, Otto-von-Guericke University Magdeburg, Germany robert.kowal@ovgu.de

[2] Marcus Prier and Oliver Speck are with the Chair of Biomedical Magnetic Resonance, Otto-von-Guericke University Magdeburg, Germany

[3] Enrico Pannicke and Ralf Vick are with the Chair of Electromagnetic Compatibility, Otto-von-Guericke University Magdeburg, Germany

[4] Robert Kowal, Marcus Prier, Enrico Pannicke, Georg Rose and Oliver Speck are involved with Research Campus *STIMULATE*, Otto-von-Guericke University, Magdeburg, SA 39106, Germany

II. METHODS

To investigate the heat induced in the body of infants during an MR procedure, a detailed setup of the patient and the excitation coil was modeled. The absorbed power was calculated by SAR simulation based on the Finite Integration Technique (FIT) [4]. Subsequently thermal simulations were performed using Pennes' Bioheat Equation [5] and were evaluated in the tissue over time.

A. Modeling

A birdcage coil was modeled with its geometries for imaging infants. It consists of 16 rungs and features a total length and diameter of $26\,\mathrm{cm}$. As a low-pass design, on each rung two capacitors were placed to tune the coil to the Larmor frequency of $63.8\,\mathrm{MHz}$. The birdcage coil was driven in quadrature and an RF shield with a diameter of $28.4\,\mathrm{cm}$ and a length of $36.6\,\mathrm{cm}$ was used as a reference point for both excitation ports. The structure was complemented by two additional hollow cylinders of FR-4, which typically serve as support for birdcage and shield, having a length of $1\,\mathrm{m}$ and a wall thickness of $2\,\mathrm{mm}$.

A heterogeneous voxel model based on an 8-week-old female infant (Helmholtz Zentrum Munich [6]), was used to simulate the absorbed power distribution and consecutive temperature rise in the human body. The infant model has a length of $56.8\,\mathrm{cm}$ and a mass of $4\,\mathrm{kg}$. With a voxel resolution of 0.85 x 0.85 x $4\,\mathrm{mm}$ (X,Y,Z) a total of 67 pre-segmented tissue types are described. The electromagnetic parameters of the tissues were generated from parameterized Cole-Cole models [7]-[9] and the required thermal parameters were taken from the database of the IT'IS Foundation [10]. The parameters were adapted and assigned to the particular segmentation of the model. The well established Pennes' Bioheat Equation [4], [11], [12] was used to model the influence of the absorbed power on the temperature change over time $\frac{\partial T}{\partial t}$ as

$$\rho c \frac{\partial T}{\partial t} = \vec{\nabla}\left(\kappa \nabla T\right) + \rho\,\mathrm{SAR} + R_B\left(T_\mathrm{B} - T\right) + Q_\mathrm{M} \quad \text{(II.1)}$$

with the density ρ, heat capacity c, thermal conductivity κ and metabolic heat generation term Q_M. Blood perfusion in the tissue was modeled by the parameter R_B with a blood temperature T_B of $37\,^\circ\mathrm{C}$ and can be seen as a compensation mechanism, while SAR as an additive term contributes to a

temperature increase. The ambient temperature was modeled conservatively at 24 °C without convective effects from air flows. The infant model was positioned head centered for a typical brain examination, as shown in the cross-sectional views in Fig. 1.

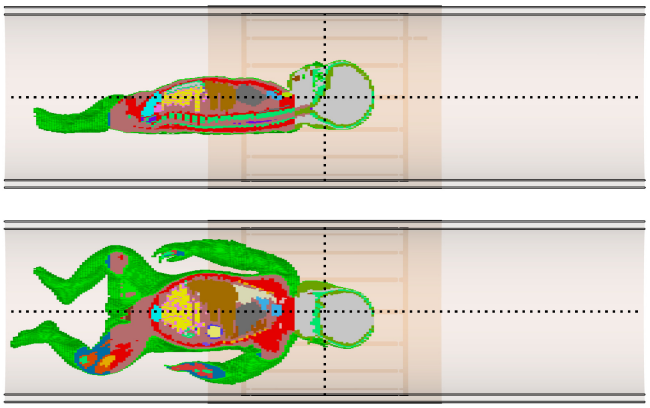

Fig. 1. Head centered position of the infant model inside the birdcage coil. Sagittal and coronal cross-sectional views.

B. SAR Simulations

Full-wave electromagnetic simulations were performed using the Finite Integration Technique (FIT) [4] in the time domain using the simulation environment CST-Studio Suite (Dassault Systèmes, France). Based on a convergence analysis with respect to the electric field in the infant and the computational resolution used, a mesh of 6 million cells was chosen. The SAR distribution was calculated in the simulation volume from the power loss and the norm-relevant SAR values in the infant model were extracted. In detail these are the SAR averaged over the whole-body (SAR_{body}), the effective partial body (SAR_{part}), the head (SAR_{head}) and the maximum local value (SAR_{local}) averaged over a 10 g element according to IEC 62704-1 [13]. The maximum permitted SAR limits [3] in normal operation mode and an averaging time of 6 min were considered and correspond to Table I. By comparing the calculated SAR values with their regulatory limits, it is possible to specify the maximum permitted RF input power. The SAR simulations, as presented

TABLE I

SAR LIMITS FOR NORMAL OPERATION MODE AND AVERAGING TIME OF 6 min [3].

SAR_{body}	SAR_{part}	SAR_{head}	SAR_{local}
2 $\frac{W}{kg}$	2-10 $\frac{W}{kg}$	3.2 $\frac{W}{kg}$	10 $\frac{W}{kg}$

in a previous study [14], show particular high absorption in the neck region, reaching levels about four times as high as the head average. Despite homogeneous excitation, the absorption shows an asymmetric profile, with a hotspot at the left neck curvature. The position of this hotspot is essentially preserved when varying the model position in the transversal plane, although its absolute intensity may fluctuate. The

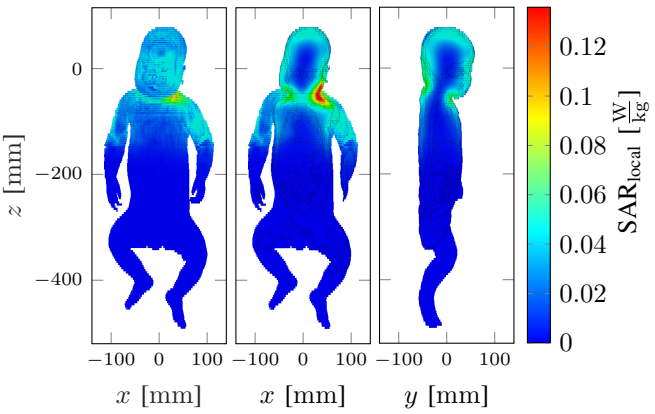

Fig. 2. SAR in the head centered infant model with a normalized 1 W input power. Frontal, coronal and sagittal views.

absorption takes place within the body volume inside of the coil and decreases rapidly inward from the periphery towards the inside of the body. These SAR distributions are also comparable to results from Malik et al. [15].

C. Thermal Simulations

The dynamic temperature distribution due to the excitation was calculated using a numerical approximation of the before mentioned bioheat equation. Regulatory limits are specified for the maximum permitted temperatures in the human body [3], as listed in Table II. The local tissue

TABLE II

TEMPERATURE LIMITS FOR NORMAL OPERATION MODE [3].

T_{core}	T_{local}	ΔT_{core}
39 °C	39 °C	0.5 °C

temperature T_{local} must not exceed 39 °C and no patient's core body temperature T_{core} must increase by more than 0.5 °C. An equilibrium state of temperature in the infant model was calculated, which establishes itself through the body's own thermal parameters without any RF excitation. This is shown in frontal and cross-sectional views in Fig. 3 and was used as the initial distribution for the excitations. A maximum of 37.6 °C was reached in the area of the heart, 37.3 °C in the brain tissue and a minimum of 36 °C at the toes. Due to the absence of air circulation, there was an additional heat radius around the body. A continuous-wave (CW) excitation amplitude was used, which has been shown to be accurate for thermal simulations without relying on the exact MR sequence [16] with an identical time-average SAR level. At its full saturation of $SAR_{local} = 10 \frac{W}{kg}$, the other regulatory limits were not yet reached, with them being at values of $SAR_{body} = 1.04 \frac{W}{kg}$, $SAR_{head} = 2.6 \frac{W}{kg}$ and $SAR_{part} = 1.91 \frac{W}{kg}$. Thus SAR_{local} represents the first of the regulatory SAR limits reached and will therefore be used as the critical value, having the most restrictive effect on the excitation.

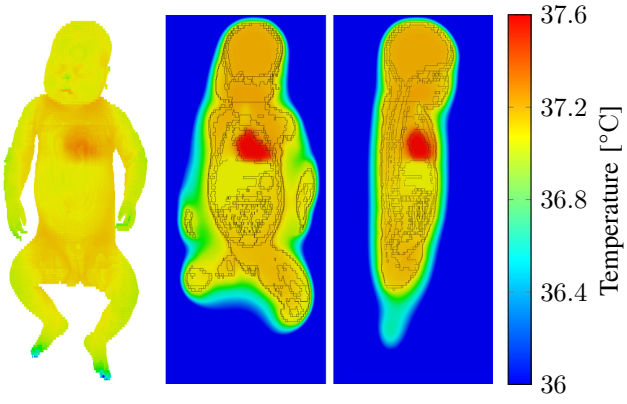

Fig. 3. Thermal equilibrium due to the intrinsic parameters of the infant model used as the initial distribution. Frontal, coronal and sagittal views.

The excitation amplitudes were scaled to result in SAR_{local} levels of $10\,\frac{W}{kg}$, $7.5\,\frac{W}{kg}$, $5\,\frac{W}{kg}$ and $2.5\,\frac{W}{kg}$, representing fractions of the SAR limit exhaustion. The temperature profile in the infant model was calculated under the exposure to the SAR levels over a period of $60\,\text{min}$. The maximum local temperature, as well as that of the brain and lungs, as critical tissues, were monitored. Both the temperature evolution and time points of exceeding critical limits were evaluated.

III. RESULTS

The increase in temperature over time for different excitation amplitudes in the infant model is presented in Fig. 4. The local SAR hotspot (see Fig. 2) resulted in the strongest temperature increase in this area. Along the neck and back area of the head, the heat spread, penetrating into deeper parts of the head over time. Other body regions which also received significant heating, but are not visible in the cross-sectional view to some extent, are spots along the upper arms at $38\,°\text{C}$ and the eyes at $37.9\,°\text{C}$, each after $10\,\text{min}$ of excitation with $SAR_{local} = 10\,\frac{W}{kg}$ ($SAR_{head} = 2.6\,\frac{W}{kg}$). The brain, as well as the lung tissue, also experienced temperature rises, which developed from the hotspot in the outermost tissues to the interior. Whereas the temperature of the heart remained almost unchanged by the excitation. The temperature rise at the neck resulting from the hotspot is shown in detail in Fig. 5 for the selected excitations over a period of $60\,\text{min}$. A flattening heating was observed, resulting from the interaction of SAR and compensatory processes as perfusion and thermal conduction. The critical value of $39\,°\text{C}$ was exceeded in the observed time at both values of $10\,\frac{W}{kg}$ and $7.5\,\frac{W}{kg}$ for SAR_{local}. This occured after a time of $t = 7\,\text{min}$ and $t = 15\,\text{min}$, respectively. An increase to more than $40\,°\text{C}$ occured for the $10\,\frac{W}{kg}$ continuous excitation after $30\,\text{min}$. The SAR of the two weaker excitations was sufficiently low that no rise of T_{local} to over $39\,°\text{C}$ was achieved within one hour. For the brain and lung tissue, the excitations with SAR_{local} values of $5\,\frac{W}{kg}$ and $2.5\,\frac{W}{kg}$ have not exceeded the limit of a $0.5\,°\text{C}$ increase. For the $10\,\frac{W}{kg}$ excitation, brain tissue reached this limit after $11\,\text{min}$ and

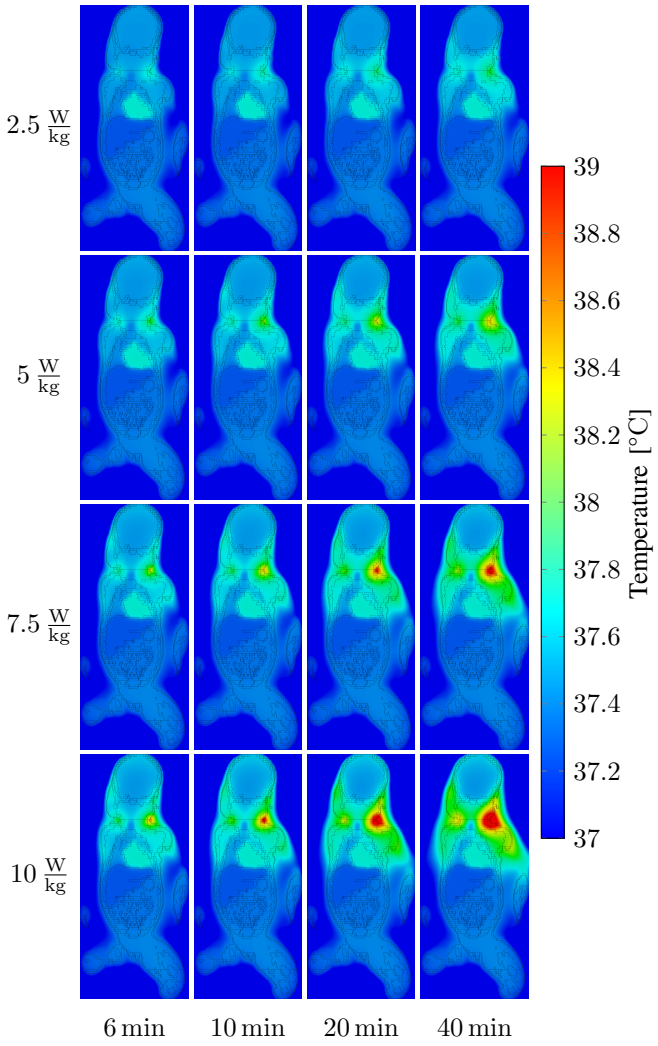

Fig. 4. Temperature at different time points in the coronal cross-section of the infant model for a head centered position. Continuous excitation amplitudes with SAR_{local} levels of $10\,\frac{W}{kg}$, $7.5\,\frac{W}{kg}$, $5\,\frac{W}{kg}$ and $2.5\,\frac{W}{kg}$.

lung tissue after $24\,\text{min}$. The $7.5\,\frac{W}{kg}$ excitation showed an exceedance for brain tissue after $21\,\text{min}$ and for lung tissue after $60\,\text{min}$. The limit exceedances are summarized by Fig. 6. The local temperature limit of $39\,°\text{C}$ was exceeded first before the deeper tissues, brain and lung, experienced an increase of $0.5\,°\text{C}$. By reducing the excitation from $10\,\frac{W}{kg}$ to $7.5\,\frac{W}{kg}$, the time intervals until the limits were exceeded, are approximately doubled.

IV. DISCUSSION

The influence of SAR on heat generation in the body of an infant in undergoing an $1.5\,\text{T}$ MRI was assessed and evaluated. The simulation results indicated that a local SAR hotspot is developed and the limit for this is reached significantly earlier than one of the more global limits. With regard to the physiologically relevant temperature, it was shown that after a certain period of time temperature limits were exceeded even if the SAR limits were respected. The

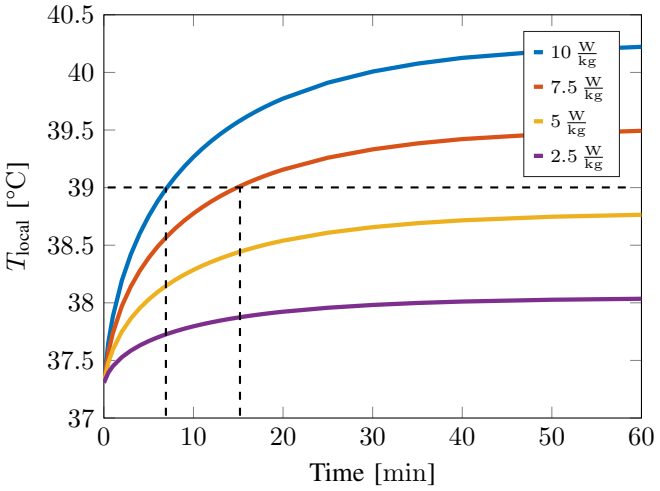

Fig. 5. Temperature at the local SAR hotspot over time for different excitation amplitudes of $\text{SAR}_{\text{local}}$. The local temperature limit is exceeded at 39 °C (dashed lines).

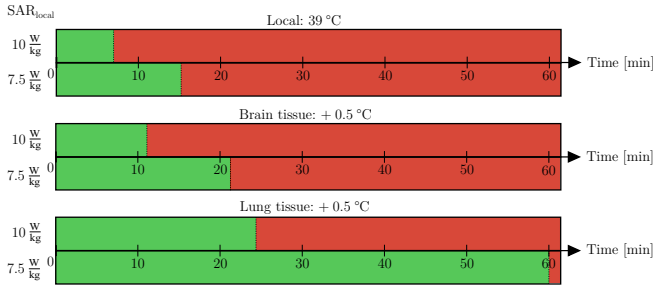

Fig. 6. Time points at which the temperature limits have been exceeded at $\text{SAR}_{\text{local}}$ levels of 10 $\frac{\text{W}}{\text{kg}}$ and 7.5 $\frac{\text{W}}{\text{kg}}$. Local (neck surface), brain and lung tissue monitored. Compliance with limit values (green), exceedance (red).

results further indicate that a thermal equilibrium has not been reached after the typical SAR averaging time of 6 min. After a period of 7 min, the temperature limit was exceeded at full exhaustion of the $\text{SAR}_{\text{local}}$ limit of 10 $\frac{\text{W}}{\text{kg}}$. The local hotspot of SAR and temperature are situated at the outer skin tissue and could be therefore argued to be tolerable. Simulated long-term exposure, however, also caused the temperature in critical organs of the body's core, such as the brain after 11 min, to exceed thresholds which must be particularly protected.

The applied patient model and its thermal response to excitation can be regarded as conservative. Thermoregulatory protective measures in healthy humans, for example, provide for an adaptive perfusion and sweating rate. In neonates and infants, however, this mechanism may not necessarily be fully developed especially in view of possible sedation [17], [18]. Additional care has to be taken with this patient group [3], as they are also unable to directly communicate any discomforts.

The specification of local SAR is not mandatory for volume coils so far. Nevertheless, it has been used as a reference in this study due to its significance, which can also be found in other publications [11], [15]. Preliminary studies indicate that the intensity of the local hotspot can vary depending on the exact excitation and patient conditions as well as their positioning. In this respect, further simulations in the scope of worst-case assumptions of the parameters or even a sensitivity analysis would be beneficial. Although this would increase complexity, it provides insight into which parameters in particular need to be most precisely defined.

In addition, initial results suggest that the relative absorption profile from a heterogeneous to a homogeneous model varies only slightly at this field strength, allowing geometrically realistic phantoms to be used for profound validation.

Apart from a general reduction of the permitted SAR, this work shows that there is no imperative equivalence between SAR and temperature limits and the importance of special constraints in the case of long-term RF-expositions. These would more strongly emphasize the temporal aspect of heating by MR sequences. With no further restrictions on short SAR limit exhausting scans, this would ensure a low-risk examination without significant thermal effects.

ACKNOWLEDGMENT

The work of this paper is partly funded by the Federal Ministry of Education and Research within the Research Campus *STIMULATE* under grant number '13GW0473A' and by the EFRE as part of R&D RF-system for neonatal MRI (project no. ZS/2018/04/91668).

REFERENCES

[1] Lancelot J. Millar et al. "Neonatal Hypoxia Ischaemia: Mechanisms, Models, and Therapeutic Challenges". In: Frontiers in Cellular Neuroscience 11, 2017, pp. 78.

[2] Donna M. Ferriero. "Neonatal Brain Injury". In: New England Journal of Medicine 351.19, 2004, pp. 1985–1995.

[3] Medical electrical equipment - Part 2-33: Particular requirements for the basic safety and essential performance of magnetic resonance equipment for medical diagnosis. Standard: 60601-2-33. Geneva, CH: International Electrotechnical Commission (IEC), 2010.

[4] T. Weiland. "A discretization model for the solution of Maxwell's equations for six-component fields". In: Archiv Elektronik und Uebertragungstechnik 31 Apr. 1977, pp. 116–120.

[5] Harry H. Pennes. "Analysis of Tissue and Arterial Blood Temperatures in the Resting Human Forearm". In: Journal of Applied Physiology 1.2, 1948, pp. 93–122.

[6] Helmholtz Zentrum Munich. German Research Center for Environmental Health. Institute of Radiation Medicine (IRM). "Virtual Human Database". 2021.

[7] K. S. Cole and R. H. Cole. "Dispersion and absorption in dielectrics: I. Alternating current characteristics." In: Journal of Chemical Physics 9, Apr. 1941, pp. 341–351.

[8] C. Gabriel and S. Gabriel. "Compilation of the Dielectric Properties of Body Tissues at RF and Microwave Frequencies". Occupational and Environmental Health Directorate, Radiofrequency Radiation Division, Brooks Air Force Base, Texas (USA), Jan. 1996.

[9] D. Andreuccetti, R. Fossi, and C. Petrucci. "An Internet resource for the calculation of the dielectric properties of body tissues in the frequency range 10 Hz - 100 GHz. IFAC-CNR, Florence (Italy). Based on data published by C.Gabriel et al. in 1996." 2021.

[10] IT'IS Foundation. "Virtual Population Database". 2021.

[11] Zhangwei Wang et al. "SAR and Temperature: Simulations and Comparison to Regulatory Limits for MRI". In: Journal of magnetic resonance imaging: JMRI26, Aug. 2007, pp. 437–441.

[12] Alireza Zolfaghari and Mehdi Maerefat. "Bioheat Transfer". In: Developments in Heat Transfer. Edited by Marco Aurélio dos Santos Bernardes. Rijeka: IntechOpen, 2011. Chapter 9.

[13] Determining the peak spatial-average specific absorption rate (SAR) in the human body from wireless communications devices, 30 MHz to 6 GHz - Part 1: General requirements for using the finite-difference time-domain (FDTD) method for SAR calculations. Standard: 62704-1:2017-10(en). Geneva, CH: International Electrotechnical Commission (IEC), Institute of Electrical and Electronics Engineers (IEEE), 2017.

[14] Robert Kowal et al. “Specific absorption rate in a dedicated birdcage coil for neonatal MRI, ESMRMB 2020 Online, 37th Annual Scientific Meeting”. In: Magnetic Resonance Materials in Physics, Biology and Medicine 33, Oct. 2020, p. 40.

[15] Shaihan J. Malik et al. “Specific absorption rate in neonates undergoing magnetic resonance procedures at 1.5T and 3T”. In: NMR in Biomedicine 28.3, Jan. 2015, pp. 344–352.

[16] Zhangwei Wang and Christopher Collins. “Effect of RF Pulse Sequence on Temperature Elevation for a Given Time-Average SAR”. In: Concepts in magnetic resonance. Part B, Magnetic resonance engineering 37B, Oct. 2010, pp. 215–219.

[17] World Health Organization (WHO). ”Environmental Health Criteria 137: Electromagnetic Fields (300 Hz to 300 GHz)”. 1993.

[18] International Comission on Non-Ionizing Radiation Protection ICNIRP. “Statement on Medical Magnetic Resonance (MR) Procedures: Protection of Patients”. In: Health Physics 87.2, 2004, pp. 197–216.